

## The Relationship between Northern Hemisphere Winter Blocking and Tropical Modes of Variability

GEREON GOLLAN

*GEOMAR Helmholtz Centre for Ocean Research Kiel, Kiel, Germany*

RICHARD J. GREATBATCH

*GEOMAR Helmholtz Centre for Ocean Research Kiel, and Faculty of Mathematics and Natural Sciences, Kiel University, Kiel, Germany*

(Manuscript received 14 October 2016, in final form 26 July 2017)

### ABSTRACT


In the present study, the influence of some major tropical modes of variability on Northern Hemisphere regional blocking frequency variability during boreal winter is investigated. Reanalysis data and an ensemble experiment with the ECMWF model using relaxation toward the ERA-Interim data inside the tropics are used. The tropical modes under investigation are El Niño–Southern Oscillation (ENSO), the Madden–Julian oscillation (MJO), and the upper-tropospheric equatorial zonal-mean zonal wind  $[U150]_E$ . An early (late) MJO phase refers to the part of the MJO cycle when enhanced (suppressed) precipitation occurs over the western Indian Ocean and suppressed (enhanced) precipitation occurs over the Maritime Continent and the western tropical Pacific. Over the North Pacific sector, it is found that enhanced (suppressed) high-latitude blocking occurs in association with El Niño (La Niña) events, late (early) MJO phases, and westerly (easterly)  $[U150]_E$ . Over central to southern Europe and the east Atlantic, it is found that late MJO phases, as well as a suppressed MJO, are leading to enhanced blocking frequency. Furthermore, early (late) MJO phases are followed by blocking anomalies over the western North Atlantic region, similar to those associated with a positive (negative) North Atlantic Oscillation. Over northern Europe, the easterly (westerly) phase of  $[U150]_E$  is associated with enhanced (suppressed) blocking. These results are largely confirmed by both the reanalysis and the model experiment.

### 1. Introduction

It is commonly accepted that the tropics influence teleconnection patterns in the extratropics, especially in the winter hemisphere (e.g., Trenberth et al. 1998; L'Heureux and Thompson 2006; Greatbatch et al. 2012) and also that enhanced skill in the tropics improves the simulation of the extratropical general circulation (e.g., Ferranti et al. 1990; Jung et al. 2010; Gollan et al. 2015). The two dominant modes of tropical variability are El Niño–Southern Oscillation (ENSO; interannual to decadal) and the Madden–Julian oscillation (MJO; intra-seasonal to interannual).

In addition to the influence on global teleconnection patterns, ENSO variability has been associated with anomalous blocking characteristics in the North Pacific region (Renwick and Wallace 1996; Wiedenmann et al. 2002; Barriopedro et al. 2006; Hinton et al. 2009; Barriopedro and Calvo 2014). Blocking, on the one hand, has major implications for local surface weather and extreme events (e.g., Trigo et al. 2004; Sillmann and Croci-Maspoli 2009; Greatbatch et al. 2015), but has also been identified in certain regions as a precursor for stratospheric anomalies like sudden warmings (e.g., Garfinkel et al. 2010; Woollings et al. 2010; Ayarzagüena et al. 2015), again allowing for a global impact of blocking. Gollan et al. (2015) have shown that the tropics as a whole significantly influence the interannual and decadal variability of midlatitude blocking frequency over the North Pacific–American and the North Atlantic–European regions and discussed tropical climate modes that exert this influence.

---

 Denotes content that is immediately available upon publication as open access.

---

*Corresponding author:* Gereon Gollan, ggollan@geomar.de

DOI: 10.1175/JCLI-D-16-0742.1

© 2017 American Meteorological Society. For information regarding reuse of this content and general copyright information, consult the [AMS Copyright Policy](http://www.ametsoc.org/PUBSReuseLicenses) ([www.ametsoc.org/PUBSReuseLicenses](http://www.ametsoc.org/PUBSReuseLicenses)).

There is general agreement on the teleconnectivity of ENSO in the North Pacific region, warm eastern Pacific El Niño events being associated with an anomalously deep Aleutian low or positive Pacific–North American (PNA) pattern (e.g., Trenberth et al. 1998; Garfinkel and Hartmann 2008), but the influence of ENSO on blocking is less clear. Contradictions in the findings concerning blocking anomalies can result from different definitions of blocking indices, with earlier studies often looking for blocking only around a fixed central latitude [one-dimensional (1D) blocking indices; e.g., Tibaldi and Molteni 1990], while more recent studies identify blocking near the climatological position of the storm track (e.g., Pelly and Hoskins 2003) or everywhere in the extratropics (2D blocking indices; e.g., Schwierz et al. 2004; Scherrer et al. 2006; Berrisford et al. 2007). In addition to this, there are many different flavors of ENSO variability, as, for example, some events can be classified as eastern Pacific or central Pacific (e.g., Garfinkel et al. 2013). Concerning classical, eastern Pacific ENSO, earlier studies found increased blocking in the subtropical northeast Pacific region associated with La Niña (vice versa for El Niño; Renwick and Wallace 1996; Wiedenmann et al. 2002; Barriopedro et al. 2006). On the other hand, Hinton et al. (2009) found, using sensitivity experiments with an atmospheric general circulation model, that cold eastern tropical Pacific sea surface temperature (SST) anomalies associated with La Niña lead to suppressed blocking in the North Pacific region, while warm SST anomalies over the Maritime Continent, also associated with La Niña, promote blocking, a duality that could be the reason for contradictory results concerning the blocking response to ENSO.

While the influence of the MJO on Northern Hemisphere teleconnections, and also some influence on the stratosphere, has been investigated quite extensively (e.g., Cassou 2008; Lin et al. 2009; Garfinkel et al. 2012b; Yoo et al. 2012a,b; Garfinkel et al. 2014; Adames and Wallace 2014; Bao and Hartmann 2014; Lin et al. 2015), the influence of the MJO on blocking has only recently been explored in some detail by a few studies. Gollan et al. (2015) found that enhanced convection over the Maritime Continent (Indian Ocean) associated with the MJO is succeeded by enhanced (decreased) blocking frequency over Europe. Further, the influence of the MJO on Northern Hemisphere winter blocking has recently been explored using reanalysis data by Henderson et al. (2016, hereinafter HMB16). Using a 2D blocking index, HMB16 analyzed anomalous blocking coinciding with (or following) MJO events and found significant changes in all of the Pacific, the Atlantic, and the European sectors. They used the Wheeler and Hendon (2004) MJO index that defines eight different phases, each phase

being associated with precipitation anomalies across the tropical regions of the Indian and Pacific Oceans, their alternation describing the eastward propagation of the MJO. HMB16 found that the strongest anomalies in midlatitude blocking for the Pacific and the Atlantic sectors follow MJO phases 3 and 7, blocking frequency being increased after MJO phase 7<sup>1</sup> and decreased after MJO phase 3.<sup>2</sup> The changes in blocking frequency over the Pacific are, according to HMB16, related to the stationary Rossby wave response to the diabatic tropical heating of the MJO, with resulting changes in storm-track propagation and poleward displacement of warm and low potential vorticity (PV) subtropical air (see also Hinton et al. 2009). The Atlantic blocking response found by HMB16 is consistent with changes in the North Atlantic Oscillation (NAO; see Woollings et al. 2008), a positive NAO thereby being associated with suppressed blocking over the northeastern Atlantic, and is also in agreement with earlier studies investigating the impact of the MJO on the NAO (Cassou 2008; Lin et al. 2009) and the northern annular mode (NAM; Zhou and Miller 2005; Yoo et al. 2012a,b). For the European sector HMB16 found the strongest blocking anomalies following MJO phases 4 (decreased blocking) and 6 (enhanced blocking). These authors suggest that, along with the possibility that the increased blocking after MJO phase 6 is a result of the positive NAO (NAO+) response after MJO phase 3 [as also suggested by Cassou (2008)], MJO phase 6 goes along with negative PNA anomalies in the North Pacific region that direct Rossby wave energy toward Europe.

Recently, the authors of the present study have found a major mode of tropical intraseasonal to interannual variability, being associated with the MJO, but also with shifts of the intertropical convergence zone (ITCZ), measured by the upper-tropospheric zonal-mean zonal wind along the equator [ $U150$ ]<sub>E</sub> (Gollan and Greatbatch 2015). The impact of [ $U150$ ]<sub>E</sub> on the extratropics includes strengthened northwest Pacific westerlies during westerly [ $U150$ ]<sub>E</sub>, a strengthening of the subtropical waveguides during easterly [ $U150$ ]<sub>E</sub>, and subtropical Rossby wave source anomalies near North America leading to an anomalous wave train across the North Atlantic. A significant correlation between seasonal mean winter blocking over Europe and [ $U150$ ]<sub>E</sub> has also been identified, westerly (easterly) [ $U150$ ]<sub>E</sub> thereby being associated with suppressed (enhanced) blocking over Europe (Gollan et al. 2015).

<sup>1</sup> MJO phase 7 is associated with enhanced convection over the western tropical Pacific.

<sup>2</sup> MJO phase 3 is associated with enhanced convection over the eastern Indian Ocean.

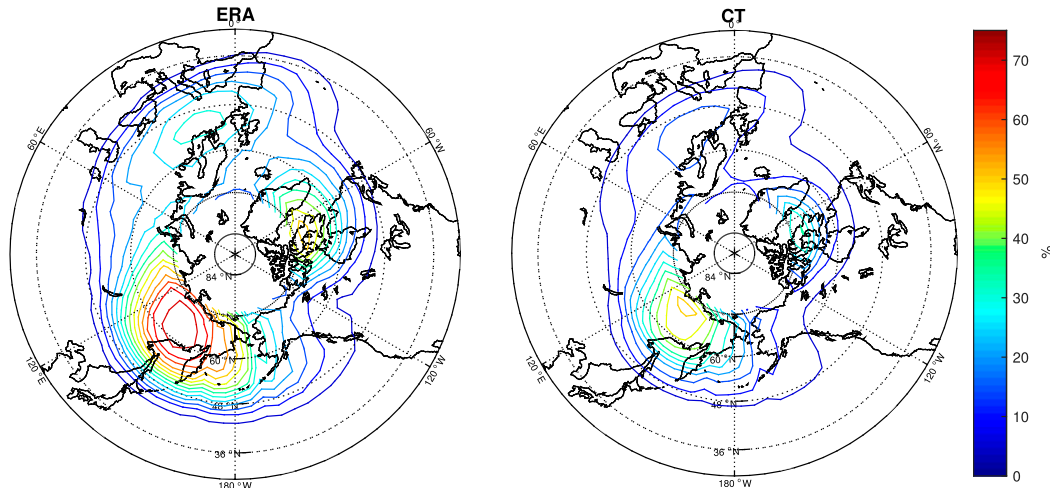


FIG. 1. DJF mean blocking frequency climatologies (i.e., fraction of all days in DJF that are part of a blocking episode) for (left) ERA and (right) CLIM-TROPICS (CT) relaxation experiment using all model realizations separately. Contour interval is 5%.

In the present paper, we will expand on the work by HMB16, by using a set of atmospheric general circulation model (AGCM) experiments where the tropics are relaxed toward European Centre for Medium-Range Weather Forecasts (ECMWF) interim reanalysis (ERA-Interim) data, but will also use the reanalysis data itself to analyze the impact of ENSO, the MJO, and  $[U150]_E$  on blocking. To this aim, we construct composites of a 2D blocking frequency index according to Woollings et al. (2008) that uses potential temperature at the tropopause level.

The paper is organized as follows: data and methods are described in section 2; the results regarding the relationship between extratropical blocking frequency and the tropical modes ENSO, MJO, and  $[U150]_E$  are presented in section 3; and a summary and discussion are given in section 4.

## 2. Data and methods

### a. Reanalysis data and model

Data are used from the 40-yr ECMWF Re-Analysis (ERA-40; Uppala et al. 2005) and ERA-Interim (Dee et al. 2011) for boreal winters [December, January, and February (DJF)] from 1960/61 to 2013/14 for all atmospheric parameters in this paper. The two datasets are combined, by using ERA-40 data until December 1978 and ERA-Interim data thereafter, the combination then being labeled as “ERA.” Sea surface temperature (SST) from the National Oceanographic and Atmospheric Administration’s (NOAA) Extended Reconstructed SST, version 3b (ERSST.v3b), dataset is used to measure ENSO variability. Additionally, we use output from a set

of relaxation experiments performed with the ECMWF Integrated Forecast System (IFS; cycle CY40R1) in its atmosphere-only setup in spectral truncation T255 (approximately 80 km), in which the dynamical atmospheric parameters<sup>3</sup> are strongly relaxed (at a time scale of 5 h) toward ERA-Interim data within the tropics<sup>4</sup> and SST and sea ice are specified to climatology, covering winters 1979/80 to 2013/14 [CLIM-TROPICS; a detailed model description and experimental setup can be found in Hansen et al. (2017)]. Although the freely running ECMWF model has, as most other models, difficulties in simulating a realistic MJO, in CLIM-TROPICS, tropical variability is relaxed toward the reanalysis data, the latter covering the satellite era (starting in 1979), so that the tropical variability, including the MJO, in the relaxation experiment can be assumed to be realistic (see Oliver 2016). The experiment CLIM-TROPICS is then used to investigate the strength of the tropically forced signal by looking at the mean blocking frequency (see section 2b for definition), obtained by averaging blocking frequency from all nine available ensemble members, to (largely) remove internal extratropical variability as represented by the model. This average blocking frequency then defines our ensemble mean, and blocking anomalies shown for CLIM-TROPICS refer to the departure of the ensemble mean from the model climatology, shown in Fig. 1b. The model blocking climatology is similar to the reanalysis climatology apart

<sup>3</sup> The dynamical parameters are zonal and meridional wind ( $u, v$ ), temperature  $T$ , and the logarithm of surface pressure  $\ln(p_s)$ .

<sup>4</sup> The relaxation coefficient reduces to zero between 10° and 30°N using a hyperbolic tangent function of latitude.

from common model biases, (i.e., the climatological blocking frequency is reduced in the model by about 20%–30% compared to the reanalysis). We note here that the reduced blocking frequency in the model results mainly from the episode criterion (see below for definition), indicating that blocking in the model is not as persistent as in observations.

### b. Blocking diagnostic

Blocking events are characterized by a deep and large-scale reversal of the prevailing westerly flow including the jet stream at mid- to high latitudes, often leading to severe weather events like the cold European winters of 1962/63 or 2005/06 (e.g., [Croci-Maspoli and Davies 2009](#); [Greatbatch et al. 2015](#)). Here we use a 2D index that is computed over the whole extratropics and can identify high-latitude blocking in addition to mid-latitude blocking most often found by 1D indices (e.g., [Tibaldi and Molteni 1990](#); [Pelly and Hoskins 2003](#)). High-latitude blocking often has a weaker imprint on flow patterns, as the climatological gradients are weaker at higher latitudes, and diverts the jet rather than blocking it. Nevertheless, high-latitude blocking can be very persistent (note in [Fig. 1](#) the climatological blocking peak over northeastern Siberia, where in the reanalysis 7 out of 10 days in DJF are characterized by blocking) and has been associated with the initiation of anomalous circulation regimes of the NAO or the west Pacific pattern that are known to have a strong surface impact (e.g., [Schwierz et al. 2004](#); [Berrisford et al. 2007](#); [Woollings et al. 2008](#)). Following [Berrisford et al. \(2007\)](#) and [Woollings et al. \(2008\)](#) we use the meridional gradient of potential temperature ( $\theta$ ) at the “dynamical tropopause” for the definition of the blocking index. This 2D blocking index identifies Rossby wave breaking, leading to a strong northward displacement of potentially warm air of low potential vorticity, the index also being known as a wave-breaking index ([Woollings et al. 2008](#)). The dynamical tropopause is defined as the surface where PV equals 2 PVU (PV2; 1 PVU =  $10^{-6}$  K m<sup>2</sup> kg<sup>-1</sup> s<sup>-1</sup>; see [Hoskins et al. 1985](#)). The index is then calculated on a 4° by 5° grid in latitude–longitude space, between 25° and 73°N. A location at longitude  $\lambda_0$  and latitude  $\phi_0$  is said to be blocked if the poleward meridional gradient of daily mean  $\theta$  at the PV2 surface ( $\theta_{\text{PV2}}$ ) is reversed (i.e., positive instead of negative). We therefore compute the difference in  $\theta_{\text{PV2}}$  between a northern and a southern box, given by

$$\Delta\theta_{\text{PV2}}(\lambda_0, \phi_0) = \int_{\lambda_0 - \Delta\lambda}^{\lambda_0 + \Delta\lambda} \left( \int_{\phi_0}^{\phi_0 + \Delta\phi} \theta_{\text{PV2}} d\phi - \int_{\phi_0 - \Delta\phi}^{\phi_0} \theta_{\text{PV2}} d\phi \right) d\lambda, \quad (1)$$

at the location  $(\lambda_0, \phi_0)$  with  $\Delta\lambda = 2.5^\circ$  and  $\Delta\phi = 15^\circ$ . The choice of  $\Delta\lambda$  and  $\Delta\phi$  follows [Woollings et al. \(2008\)](#), but the results shown below are not sensitive to slight changes of these parameters. To account for slight meridional movement of blocking systems, the calculation is repeated replacing  $\phi_0$  by  $\phi_0 \pm 4^\circ$  and retaining only the maximum of the three values. This instantaneous blocking index is then set to one when  $\Delta\theta_{\text{PV2}}$  is positive and to zero otherwise. Large-scale events are selected by only retaining instantaneous blocking extending over at least 15° of longitude. Then, considering each grid point separately, a blocking episode is said to occur when large-scale blocking occurs within a zonal range of 10° of that grid point for at least five consecutive days. From the resulting daily binary time series of blocking episodes for DJF, blocking frequency composites are computed corresponding to the ENSO, MJO, or  $[U150]_E$  indices (see below for definition). In the following, reanalysis anomalies refer to deviations from the DJF climatology of the ERA reanalysis (1960/61 to 2013/14; shown in [Fig. 1a](#)) and model anomalies refer to deviations from the DJF model climatology for all simulated winters (1979/80 to 2013/14; see [Fig. 1b](#)).

To test the statistical significance of the blocking composites according to the selected climate indices we perform Monte Carlo tests for each index, shuffling the blocking frequency anomalies in time to create artificial realizations ( $n = 4000$ ). Thereby, seasons and months are viewed as independent from each other, and for daily blocking frequency, periods of 10 consecutive days from the original data are randomly concatenated (allowing overlap) to create 4000 artificial daily time series of blocking frequency that have the same length as the original data. With these artificial time series of blocking frequency anomalies, composites are computed using the original climate indices. At each grid point we choose the 2.5th and 97.5th percentile of the resulting blocking frequency probability distribution as our significance thresholds.<sup>5</sup> This procedure is chosen instead of a Student’s  $t$  test because the blocking frequency distribution at many locations is non-Gaussian and also the climate indices may be nonnormal.

### c. Definition of climate indices

#### 1) Niño-3.4

As a measure for ENSO variability, we use the DJF seasonal mean Niño-3.4 index, which is the area average of SST anomalies over the region 170° to 120°W and 5°S

<sup>5</sup> We do not plot significance on grid points, where the 2.5th and 97.5th percentiles are separated by a blocking frequency of less than 4% (2% for the model).



to 5°N, using the ERSST.v3b dataset here. The mean and standard deviation of the DJF mean Niño-3.4 index for the period 1960/61–2013/14 are 26.6°C and 1.03 K, respectively.

## 2) MJO

The daily MJO index, defined by [Wheeler and Hendon \(2004\)](#), is used and was downloaded from the home page of the website of the Australian Bureau of Meteorology.<sup>6</sup>

This MJO index consists of two components, RMM1 and RMM2, that are the first two principal components from a multivariate empirical orthogonal function (EOF) analysis on tropical zonal wind at 850 and 200 hPa, as well as on outgoing longwave radiation, which is continuously available only during the satellite era after 1979. Before the EOF analysis, the seasonal cycle is removed from all variables. Both indices are normalized by their respective standard deviations, and eight MJO phases are defined by the angle of the vector that is spanned by the two components, while the MJO amplitude is defined as the length of the following vector:  $|\text{RMM1}, \text{RMM2}| = [(\text{RMM1})^2 + (\text{RMM2})^2]^{1/2}$ .

## 3) $[U150]_E$

As in [Gollan and Greatbatch \(2015\)](#) we use the zonal-mean zonal wind  $[U]$ , area averaged between 5°S and 5°N at 150 hPa for DJF monthly means. Because this time series is weakly correlated with the monthly mean Niño-3.4 index, we remove that part of variability that is linearly dependent on the Niño-3.4 index and subsequently remove the seasonal cycle by subtracting from each month the climatological monthly mean, the resulting index being called  $[U150]_E$ . When the daily  $[U150]_E$  index is used, the part of variability linearly dependent on the monthly mean Niño-3.4 index, as removed from the monthly mean  $[U150]_E$ , is removed from the daily time series (there are no discontinuities in the resulting index, as the influence of Niño-3.4 is small compared to the variability of the daily  $[U150]_E$  index). Furthermore, while the 10-day low-pass-filtered daily climatology is subtracted from the daily index. The standard deviation of  $[U150]_E$  before normalization is  $2.5 \text{ m s}^{-1}$  for the monthly and  $3.7 \text{ m s}^{-1}$  for the daily time series, while the mean of  $[U150]_E$  is  $1.5 \text{ m s}^{-1}$ . In the case of composites according to the daily  $[U150]_E$ , only events persisting at least 8 days are retained to focus on the stronger-than-average events (7 days on average), and, for each anomalous phase of  $[U150]_E$ , the central

date is used for the generation of composites. If the length of the anomalous period is an even number, the last day of the first half of the period is used as a central date (“peak”) in the daily index.

All indices in this study (except the MJO index, which is used as is) are linearly detrended before the analysis to focus on intraseasonal to interannual time scales, although [Barnes et al. \(2014\)](#) point out that the observed trends in blocking frequency are not significant compared to interannual and decadal variability. Also, all indices are normalized, (i.e., the time mean is removed and the resulting index is divided by its standard deviation). Composites are then computed by averaging blocking frequency over months (or days) when the respective index exceeds plus/minus one standard deviation.

## 3. Relationship between tropical variability and extratropical blocking

### a. *El Niño–Southern Oscillation*

The canonical teleconnection associated with ENSO is the PNA pattern (e.g., [Trenberth et al. 1998](#); [Garfinkel and Hartmann 2008](#)), with an anomalously deep (shallow) Aleutian low during El Niño (La Niña) events. Some studies found significantly enhanced (suppressed) blocking during La Niña (El Niño) over the North Pacific, but some of these studies found the signal in the midlatitudes ([Renwick and Wallace 1996](#); [Wiedenmann et al. 2002](#)), where our index identifies very few blocking episodes in general (see [Fig. 1](#)), and only a more recent study focused on the higher latitudes ([Barriopedro and Calvo 2014](#)). However, [Hinton et al. \(2009\)](#) found opposite dipoles in geopotential height over the North Pacific being driven by idealized La Niña-like SST forcing in an AGCM, favoring blocking in the case of warm SST over the Maritime Continent and suppressing blocking in the case of cold SST over the eastern tropical Pacific. Consequently, [Hinton et al. \(2009\)](#) note that the overall impact of ENSO on North Pacific blocking depends on the relative magnitude of the SST anomalies in the two regions during individual events.

[Figure 2](#) shows the seasonal mean blocking frequency anomalies composited according to winters associated with El Niño and La Niña separately, for the reanalysis<sup>7</sup> and for the tropical relaxation experiment.<sup>8</sup> Different from [Barriopedro and Calvo \(2014\)](#), we find enhanced blocking over the eastern North Pacific (up to 8%) during El Niño winters and decreased blocking over

<sup>6</sup> <http://www.bom.gov.au/climate/mjo/graphics/rmm.74toRealtme.txt>.

<sup>7</sup> El Niño winters: 1965/66, 1972/73, 1982/83, 1986/87, 1991/92, 1994/95, 1997/98, 2002/03, and 2009/10. La Niña winters: 1970/71, 1973/74, 1975/76, 1988/89, 1998/99, 1999/2000, 2007/08, and 2010/11.

<sup>8</sup> Only events after 1979/80 apply for the model.

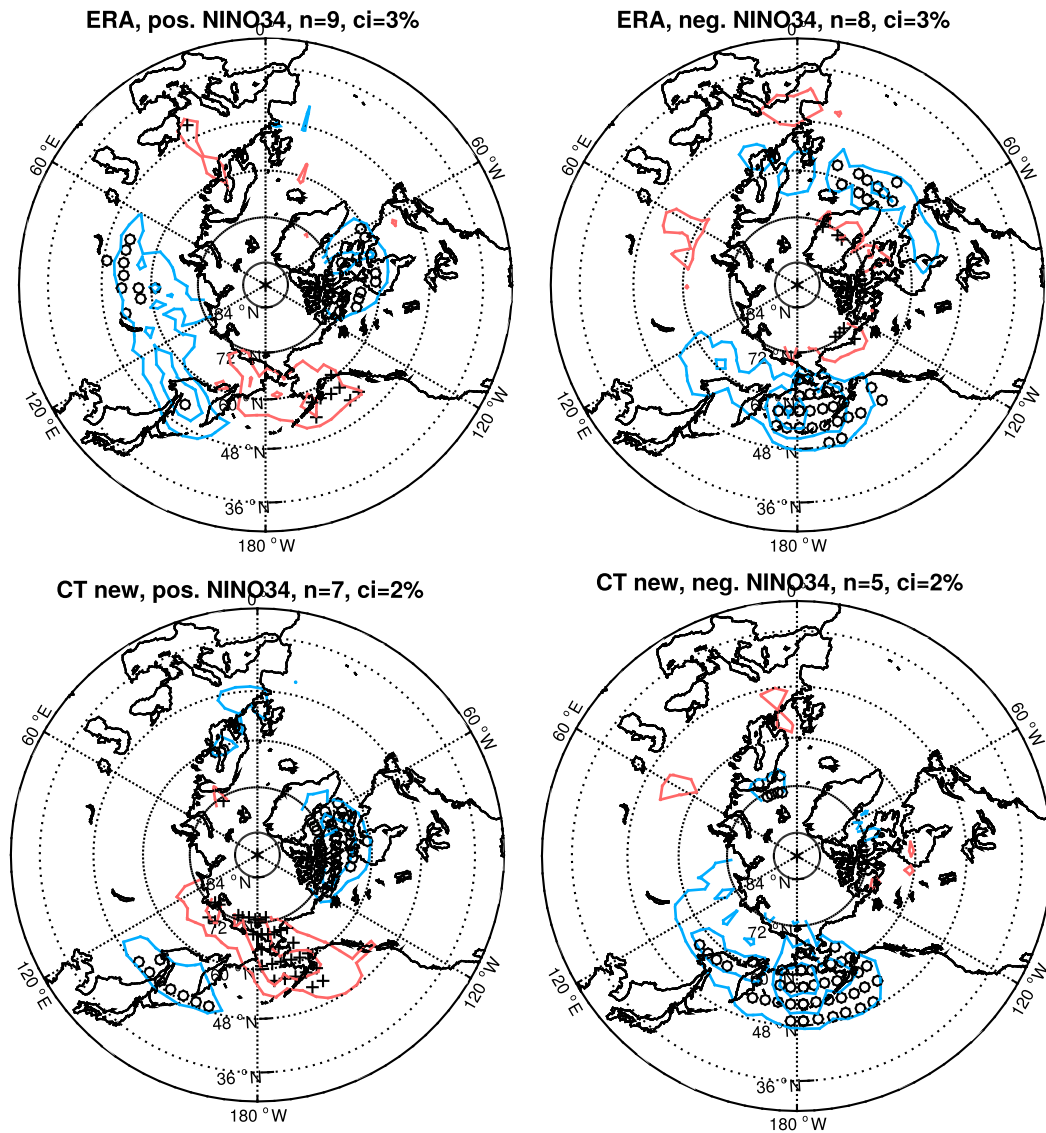


FIG. 2. Anomalous blocking frequency composited according to winters (DJF) with anomalous (left) El Niño and (right) La Niña for (top) ERA (1960/61 to 2013/14<sup>7</sup>) and (bottom) CLIM-TROPICS (1979/80 to 2013/14<sup>8</sup>; see text for more details). Red (blue) colors indicate enhanced (decreased) blocking frequency, and contours are drawn every 4% (2%) for ERA (CT), the zero contour being omitted. Plus (circle) symbols indicate significant values [i.e., > (<) the 97.5th (2.5th) percentile according to a Monte Carlo test]. The number of seasons used to calculate the respective composite is given as  $n$  in the title of each panel.

northern Canada/Hudson Bay (up to 8%), very similar in both the reanalysis and the ensemble mean of CLIM-TROPICS, even in terms of the amplitude of the blocking anomalies. It is fairly unusual to see a signal in the ensemble mean being of the same amplitude as in observations,<sup>9</sup> giving strong confidence in the signal

here. There is also a reduction of blocking frequency (up to 8%) over the western North Pacific and over Siberia during El Niño that, together with the enhanced blocking over the Aleutians, forms a dipole suggesting a northeastward shift of the climatological Siberian blocking peak.

The blocking anomalies for La Niña conversely indicate reduced blocking frequency over the Aleutians in both the reanalysis and the model but are missing the dipole over the western North Pacific. There is also a

<sup>9</sup>Note that the model anomalies are plotted at only half of the contour interval as the reanalysis anomalies.

weak increase in blocking over the subtropical eastern North Pacific during La Niña, consistent with [Renwick and Wallace \(1996\)](#) and [Wiedenmann et al. \(2002\)](#), but the blocking anomalies are below our lowest plotted contour interval. Therefore, our results emphasize the impact of ENSO on blocking at high latitudes instead of subtropical latitudes. Furthermore, there is a significant decrease in blocking frequency (up to 8%) for La Niña over the western North Atlantic (only in the reanalysis), characteristic of NAO+ (following [Woollings et al. 2008](#)), consistent with previous studies (e.g., [Brönnimann 2007](#)). Additionally, both the reanalysis and the relaxation experiment indicate slightly increased blocking frequency over central and southern Europe for La Niña winters, possibly related to anticyclonic wave breaking as during NAO+ events.

We note here that the enhanced (suppressed) blocking over the eastern North Pacific during El Niño (La Niña) winters is consistent with the stationary Rossby wave response to ENSO—that is, a deepened and southward-shifted (more shallow and northward shifted) Aleutian low during El Niño (La Niña) that reduces (enhances) the meridional gradient of geopotential height on the northern flank of the anomaly, in line with the argumentation of [Hinton et al. \(2009\)](#) but disagreeing with [Barriopedro and Calvo \(2014\)](#). It might be worth noting that the climatology of the blocking index used by [Barriopedro and Calvo \(2014\)](#); cf. Fig. 4 in [Schwierz et al. 2004](#)) differs substantially from the climatology of the blocking index used here (see [Fig. 1](#)), a possible explanation for the difference in the ENSO composites.

Enhanced blocking over the eastern North Pacific has been identified as a precursor for stratospheric polar vortex splitting (weakening) events ([Martius et al. 2009](#)), whereas northward shifts of blocking over the western North Pacific (as seen here for the model during El Niño) have been identified as precursors of intensified stratospheric polar vortex regimes ([Woollings et al. 2010](#)). In the end, sudden stratospheric warming (SSW) frequency [measured by the algorithm of [Charlton and Polvani \(2007\)](#)] is enhanced during both El Niño and La Niña winters in both the reanalysis and in the model,<sup>10</sup> consistent with [Garfinkel et al. \(2012a\)](#) and [Barriopedro and Calvo \(2014\)](#). Nevertheless, the increased SSW frequency during ENSO winters does not enhance seasonal mean blocking anomalies over the western

North Atlantic as could be inferred from the stratospheric downward influence on the NAO noted by previous studies (e.g., [Ineson and Scaife 2009](#)). [Woollings et al. \(2010\)](#) also showed that SSWs are followed by increased blocking over the Pacific basin, potentially offering a positive feedback from the stratosphere supporting the enhanced blocking over the eastern North Pacific seen for El Niño (but not for La Niña).

### b. Madden–Julian oscillation

As summarized in the introduction, [HMB16](#) investigated the influence of the MJO on Northern Hemisphere winter blocking. Our analysis is very similar to the analysis by [HMB16](#), although here 1) we use a slightly longer time series of blocking (December 1979 to February 2014 instead of December 1979 to February 2010), 2) we use  $\theta_{pV2}$  to compute the 2D blocking index instead of 500-hPa geopotential height, and, 3) in addition to the reanalysis data, we also have model output to gain confidence in the results. Furthermore, we add the case of the suppressed MJO to the analysis. [Gollan et al. \(2015\)](#) found that the influence of the MJO on midlatitude blocking is relatively weak on interannual time scales but that on weekly time scales, early (late) MJO phases are associated with weakened (strengthened) blocking over Europe, consistent also with [Cassou \(2008\)](#). Early MJO phases (1–4) correspond to enhanced convection over the Indian Ocean and suppressed convection over the Maritime Continent, while late MJO phases (5–8) correspond to enhanced convection over the Maritime Continent and the western tropical Pacific and suppressed convection over the Indian Ocean. While both [Cassou \(2008\)](#) and [HMB16](#) found the strongest increase in blocking over Europe following MJO phase 6, [Cassou \(2008\)](#) related the increase in blocking after MJO phases 3–4 to the increased occurrence of NAO+ regimes. [HMB16](#) additionally identified a role for a negative PNA pattern prior to the occurrence of MJO phase 6 that redirects Rossby wave energy toward Europe.

We show blocking frequency anomalies averaged over days 8 to 12 (labeled as lag 10 in the following) after the occurrence of each of the eight MJO phases when active (active meaning that  $|\text{MJO}| \geq 1.5$ ) in [Fig. 3](#) for the reanalysis and in [Fig. 4](#) for CLIM-TROPICS. Time lags 5, 10, and 15 are given for MJO phase 6 in [Fig. 5](#), for the reanalysis only, showing that a 10-day lag is a reasonable time scale for anomalies driven by the MJO to reach the European sector. In the reanalysis, blocking frequency is increased strongly over the western North Atlantic after MJO phase 7, similar to negative NAO-like (NAO–)

<sup>10</sup> Average number of SSWs per winter (DJF) in ERA: 0.68 (El Niño), 0.58 (La Niña), and 0.37 (neutral). In CLIM-TROPICS: 0.86 (El Niño), 0.60 (La Niña), and 0.48 (neutral).

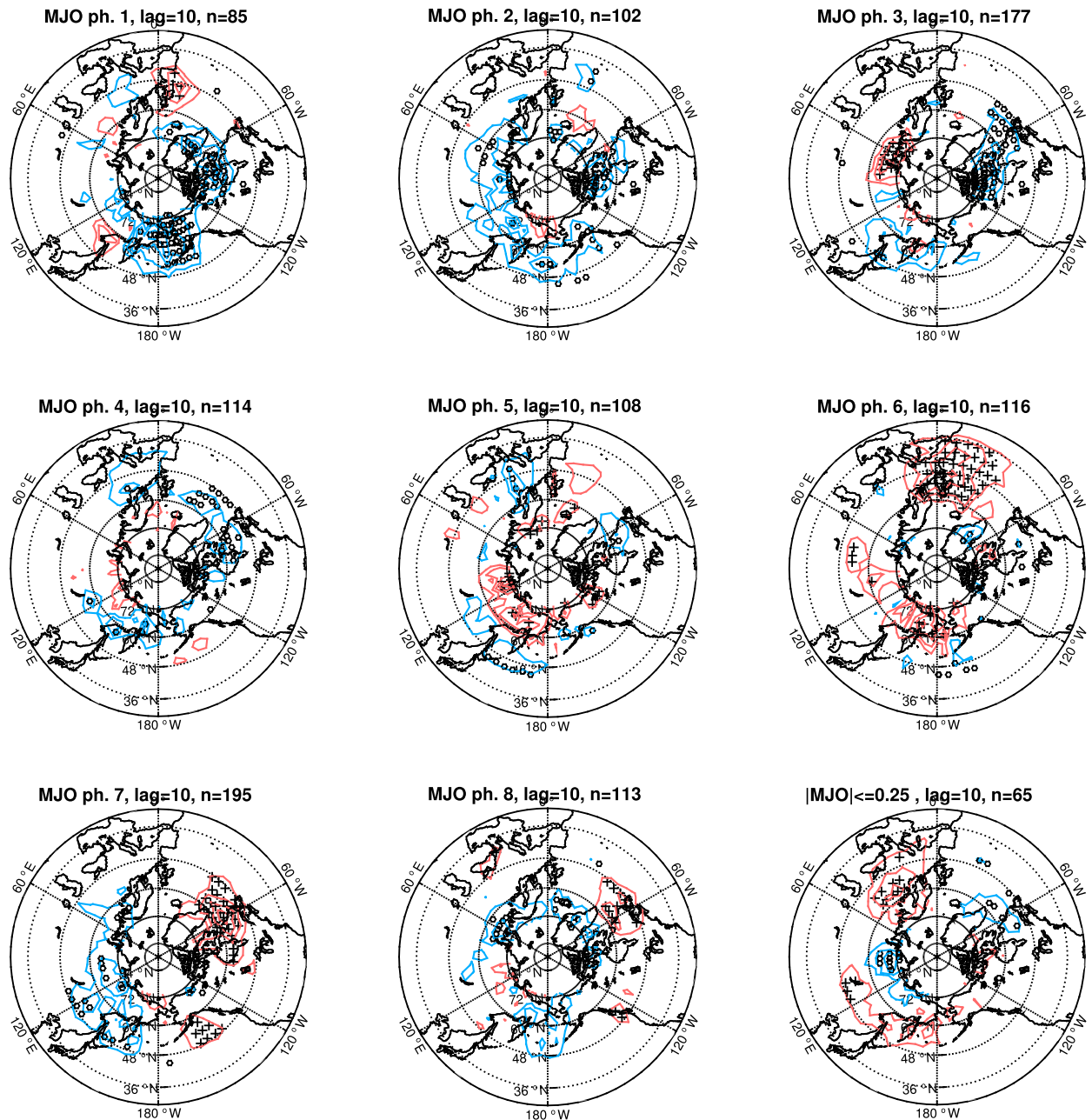


FIG. 3. (top left to bottom middle) Blocking frequency anomalies averaged over days 8 to 12 (phase 1 to 8) after days that are characterized by the respective MJO phase with sufficient amplitude,  $|MJO| \geq 1.5$ . Red (blue) colors indicate enhanced (decreased) blocking frequency. (bottom right) The respective composite according to a suppressed MJO ( $|MJO| \leq 0.25$ ). Winter months (DJF) are used for the period 1979/80–2013/14, while blocking data is from ERA-Interim and the MJO index used is the [Wheeler and Hendon \(2004\)](#) index. Contour interval is 4%, and the number of dates going into the composite (i.e., active MJO of the given phase and suppressed MJO) is given in each panel. Plus (circle) symbols indicate significant values [i.e.,  $>$  ( $<$ ) the 97.5th (2.5th) percentile according to a Monte Carlo test].

blocking anomalies (see [Woollings et al. 2008](#)). In the model, the NAO– signal is present after all of the MJO phases 6–8, but extending over a smaller region and shifted to the northwest compared to the reanalysis. Furthermore, North Atlantic blocking anomalies

following MJO phases 3 and 4 (only phase 3 in the model) are similar to the blocking anomalies associated with NAO+ (i.e., less blocking over the western North Atlantic; see [Woollings et al. 2008](#)). These findings are consistent with [Cassou \(2008\)](#), who found



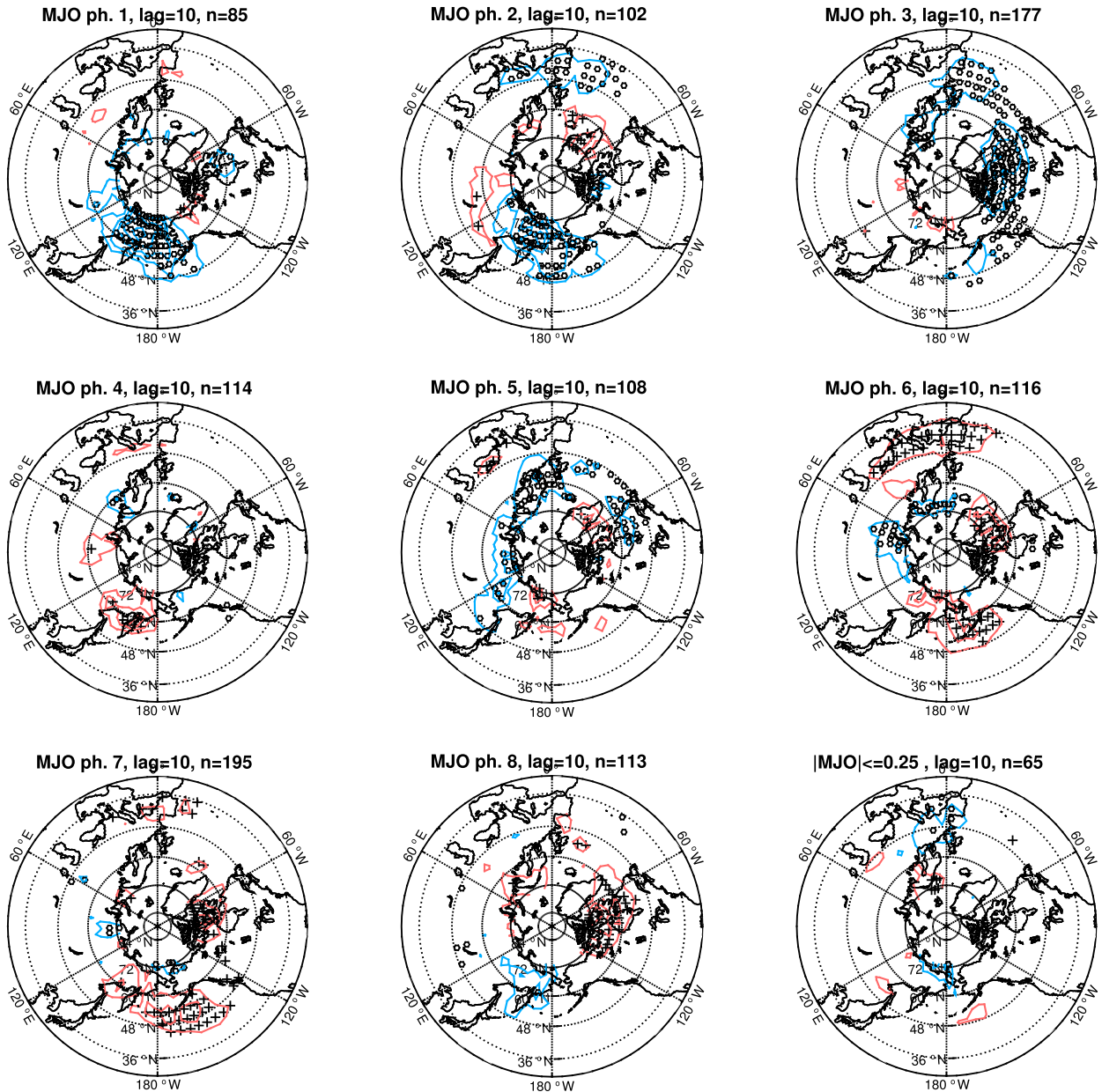


FIG. 4. As in Fig. 3, but for CLIM-TROPICS. Blocking anomalies are multiplied by a factor of 2 to give a similar amplitude compared to Fig. 3.

the probability for NAO+ (NAO−) to be increased 10 days after the occurrence of MJO phase 3 (phase 6).

The findings by Gollan et al. (2015) and HMB16 concerning European blocking are largely confirmed here, as blocking is reduced after an early MJO (after phase 4 in the reanalysis, after phases 2 and 3 in the model), the signal being slightly weaker than in HMB16. In the reanalysis (after phase 4) and in the model (after phase 3), the reduced blocking over Europe goes along with reduced blocking over the North Atlantic extending upstream to the western North Atlantic,

where reduced blocking is characteristic of NAO+, as noted above. Furthermore, in the reanalysis, blocking over Europe and the eastern North Atlantic is enhanced after late MJO phases, especially after MJO phase 6, while in the model the increase in blocking over Europe is more confined to southern Europe. The NAO-like increase in blocking over the western North Atlantic following MJO phase 7 occurs after the blocking over Europe associated with MJO phase 6, suggesting that European blocking can induce NAO− regimes upstream. Additionally, blocking frequency is reduced

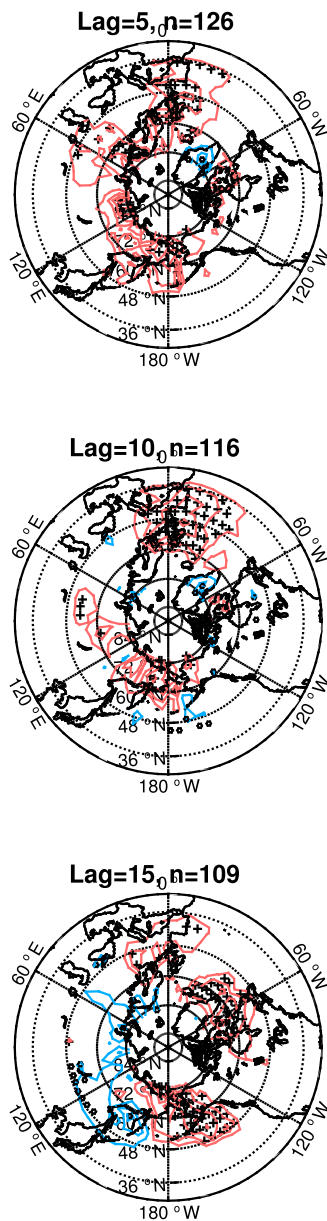


FIG. 5. As in Fig. 3, but for MJO phase 6 only and for time lags (top)–(bottom) of 5 to 15 days.

(enhanced) over almost all the Northern Hemisphere after the occurrence of MJO phases 1–3 (phases 6–7), such as one would expect in association with a positive (negative) NAM in both the reanalysis and model. Previous studies on the NAO/NAM found a similar relationship (see discussion in section 4; Zhou and Miller 2005; L’Heureux and Higgins 2008; Yoo et al. 2012a,b; Lin et al. 2015; Dahlke 2015).

We also note here the strong decrease in blocking over the (western) North Pacific following MJO phase 1 and 2 (in both the reanalysis and the model), which coincides

with the region where Garfinkel et al. (2014) identified negative sea level pressure anomalies as precursors for SSWs [and, inversely but consistently, Woollings et al. (2010) found intensified polar vortex regimes after enhanced blocking]. Moreover, blocking frequency is increased over the western North Pacific following MJO phase 6 (6 and 7 in the model), consistent with Adames and Wallace (2014) and Bao and Hartmann (2014). These authors point out that, when the MJO heating is centered over the Maritime Continent (like in phase 6), the flanking Rossby waves lead to negative geopotential height anomalies in the central subtropical North Pacific region, decreasing the climatological gradient north of the anomaly. These authors also suggest that the flanking subtropical Rossby waves associated with late-MJO-like heating can induce poleward-propagating wave trains when they reach the climatological jet-exit region. Both facts are consistent with the increased blocking frequency for late MJO phases found here and with decreased blocking frequency for early MJO phases when inverting the sign of the heating.

We also show the blocking frequency anomalies following a suppressed MJO ( $|MJO| \leq 0.25$ ) in the bottom-right panels of Figs. 3 and 4. Suppressed MJO means that precipitation in the tropics is close to climatology that is, in fact, characterized by a zonally asymmetric dipole in the MJO region with strong precipitation over the Maritime Continent and weak precipitation over the western Indian Ocean and Africa (e.g., Adler et al. 2003). While this zonal dipole is known to be an important driver of the tropical circulation and especially of the zonal-mean wind along the equator (see, e.g., Kraucunas and Hartmann 2005), a suppressed MJO leads to easterly anomalies in the zonal-mean zonal wind along the equator, which can itself have an extratropical impact [see Gollan and Greatbatch (2015) and next section]. Associated with a suppressed MJO there is, in the reanalysis, enhanced blocking frequency over central and eastern Europe (up to 12%), while in the model there is slightly decreased blocking over Europe for the suppressed MJO. The blocking anomalies associated with a suppressed MJO in the reanalysis bear slight resemblance to the blocking anomalies associated with MJO phase 6, which is associated with precipitation anomalies that amplify the climatological diabatic heating dipole. The disagreement between reanalysis and model regarding the blocking response to a suppressed MJO suggests that different features of the MJO might have an opposing extratropical impact (see next section).

### c. Upper-tropospheric zonal-mean zonal wind along the equator

The monthly mean or seasonal mean upper-tropospheric zonal-mean zonal wind along the equator

$[U1\hat{5}0]_E$  is both an expression of the preferred location of the MJO-related diabatic heating and of the meridional anomalous position of the ITCZ,<sup>11</sup> and previous studies found a statistically robust signal in the Northern Hemisphere extratropical circulation associated with  $[U1\hat{5}0]_E$  (Lee et al. 2007; Gollan and Greatbatch 2015; Gollan et al. 2015). Interestingly, while Gollan and Greatbatch (2015) found the most robust anomalies in monthly mean geopotential height over the North Pacific, Gollan et al. (2015) found a significant blocking signal over Europe, namely, decreased (enhanced) seasonal mean winter blocking frequency during westerly (easterly)  $[U1\hat{5}0]_E$ .

Figure 6 shows the anomalous 2D blocking frequency during months of anomalously westerly and easterly  $[U1\hat{5}0]_E$  during boreal winter<sup>12</sup> for reanalysis data (upper panels) and the tropical relaxation experiment (lower panels). The strongest change in blocking frequency associated with  $[U1\hat{5}0]_E$  occurs in the western North Pacific and eastern Siberian region, consistent with the regressions of monthly mean 500-hPa geopotential heights (see Gollan and Greatbatch 2015). In the reanalysis, blocking occurs more frequently over the North Pacific and over northeastern Siberia during the westerly phase of  $[U1\hat{5}0]_E$ , but this signal is not present in the model. Associated with the easterly phase of  $[U1\hat{5}0]_E$  is a north–south dipole in blocking anomalies with reduced blocking frequency over the Bering Strait and enhanced blocking over a band at midlatitudes from northern China into the North Pacific, indicating a southward shift of blocking that is present in both reanalysis and the model. The enhanced blocking over the North Pacific during westerly  $[U1\hat{5}0]_E$  is similar to the anomalies after MJO phases 5–7 (see Fig. 3), these MJO phases favoring the westerly phase of  $[U1\hat{5}0]_E$  [see discussion in Gollan and Greatbatch (2015)]. This suggests that the extratropical impacts of  $[U1\hat{5}0]_E$  and MJO either interfere constructively in the North Pacific region or are two manifestations of one phenomenon.

Over the European sector, blocking frequency is reduced during the westerly phase and slightly enhanced during the easterly phase (over the British Isles, albeit not statistically significant),<sup>13</sup> consistent with the findings

of Gollan et al. (2015) that seasonal mean blocking over Europe is negatively correlated with  $[U1\hat{5}0]_E$ . The reduction of blocking frequency over Europe during westerly  $[U1\hat{5}0]_E$  is contrary to the strengthened blocking after late MJO phases that have been associated with the westerly phase of  $[U1\hat{5}0]_E$  by Gollan and Greatbatch (2015). This difference suggests that the extratropical impact of  $[U1\hat{5}0]_E$  and the MJO can interfere destructively but could also be an indication of influences other than the MJO on  $[U1\hat{5}0]_E$ , a candidate being meridional shifts of the ITCZ (similar for easterly  $[U1\hat{5}0]_E$  vs early MJO phases).

To investigate the blocking anomalies associated with  $[U1\hat{5}0]_E$  on shorter time scales, we show the pentad mean blocking anomalies averaged over days 3 to 7 (one-pentad lag) after the central dates (peaks) in the daily  $[U1\hat{5}0]_E$  index and over days 8 to 12 (two-pentad lag) after the peaks—for the reanalysis (Fig. 7) and for the relaxation experiment (Fig. 8). Over the North Pacific, results are very similar on these shorter time scales compared to the monthly means, the signals being strongest for short lag. As such, for westerly  $[U1\hat{5}0]_E$ , the relaxation experiment indicates an eastward shift in blocking over the western North Pacific rather than an intensification as seen in the reanalysis, and for easterly  $[U1\hat{5}0]_E$  a westward shift in blocking rather than the southward shift as seen in the reanalysis. Over Europe, the signals are quite weak on short time scales, although the sign of the anomalies (for both the reanalysis and the model) confirm the results from the monthly mean analysis. We also identify some significant increase in blocking over the western North Atlantic one and two pentads after easterly peaks of  $[U1\hat{5}0]_E$ , similar to that associated with NAO– (Woollings et al. 2008), that is not present for monthly means.

The enhanced blocking over northern Europe associated with easterly  $[U1\hat{5}0]_E$  is weak on daily time scales and strong in monthly means, while the NAO-like signal for easterly  $[U1\hat{5}0]_E$  is only present in pentad means. The longer time scales for the signal over Europe suggest that slow changes in the background mean flow in association with  $[U1\hat{5}0]_E$  (see Fig. 8 in Gollan and Greatbatch 2015) are important, leading to a stronger connection between the Rossby waveguides of the Pacific and the Euro-Atlantic sectors during easterly  $[U1\hat{5}0]_E$ . The shorter time scales for the NAO– signal for easterly  $[U1\hat{5}0]_E$  on the other hand suggest that faster fluctuations (e.g., of subtropical Rossby wave source anomalies associated with  $[U1\hat{5}0]_E$ ) are important (see Fig. 9 in Gollan and Greatbatch 2015). We suggest that further work is needed to disentangle the exact mechanisms.

<sup>11</sup> An active MJO, late MJO, or an ITCZ close to the equator favor westerly  $[U1\hat{5}0]_E$ , while a suppressed MJO, early MJO, or a poleward-displaced ITCZ favor easterly  $[U1\hat{5}0]_E$ .

<sup>12</sup> Here, the monthly blocking anomalies refer to the seasonal mean climatology.

<sup>13</sup> Over Europe, the relaxation experiment confirms the reanalysis, the signal only being statistically significant in the case of easterly  $[U1\hat{5}0]_E$ .

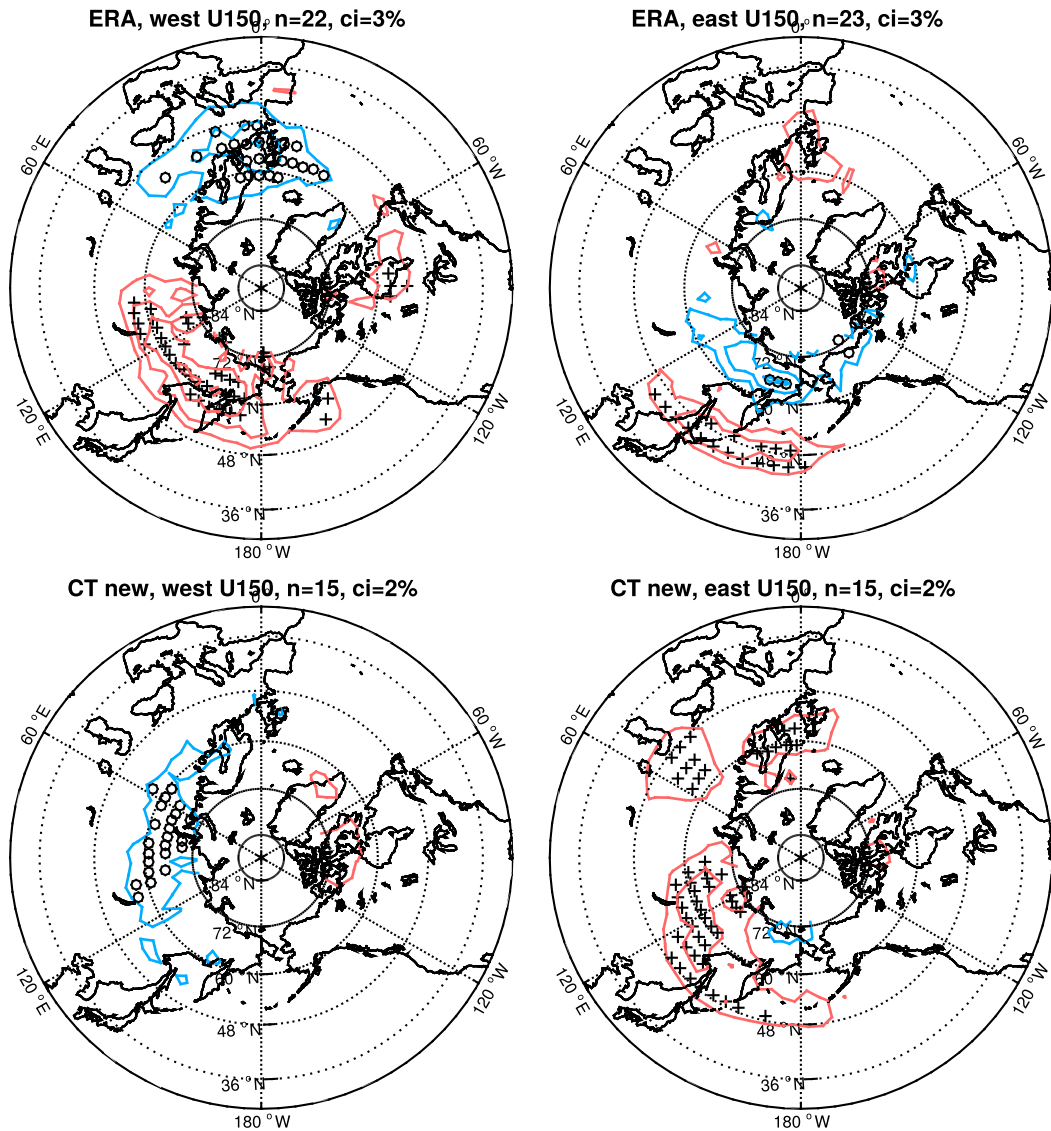


FIG. 6. Anomalous blocking frequency composited over months (DJF) with anomalously (left) westerly  $[U150]_E$  and (right) easterly  $[U150]_E$  for (top) ERA and (bottom) CT. Anomalies refer to the seasonal mean blocking climatology shown in Fig. 1. Otherwise, as in Fig. 2.

#### 4. Summary and discussion

Gollan et al. (2015) have shown that the tropics as a whole have a significant impact on boreal winter mid-latitude blocking over the Northern Hemisphere. In the present paper, the influence of some tropical modes on mid- and high-latitude blocking has been investigated using a 2D blocking index rather than the 1D index used by Gollan et al. (2015). Results for the combined ERA-40 and ERA-Interim reanalysis data (ERA) were compared with results from a model using relaxation toward ERA-Interim data in the tropics. Our model is the ECMWF seasonal Integrated Forecast System (IFS)

in an atmosphere-only setup, where the model is strongly relaxed toward reanalysis data (ERA-Interim; 1979/80–2013/14) within the tropics during the course of the seasonal forecast so that the tropics, including the MJO, in the model are close to observations. The results are summarized briefly in Table 1.

For the warm phase of ENSO (measured here by the DJF mean Niño-3.4 index), an increase in high-latitude blocking frequency over the North Pacific was shown (suppressed blocking for cold ENSO). While this finding is contrary to the findings of Barriopedro and Calvo (2014), the ENSO blocking signal over the North Pacific is underpinned by the model experiment CLIM-TROPICS



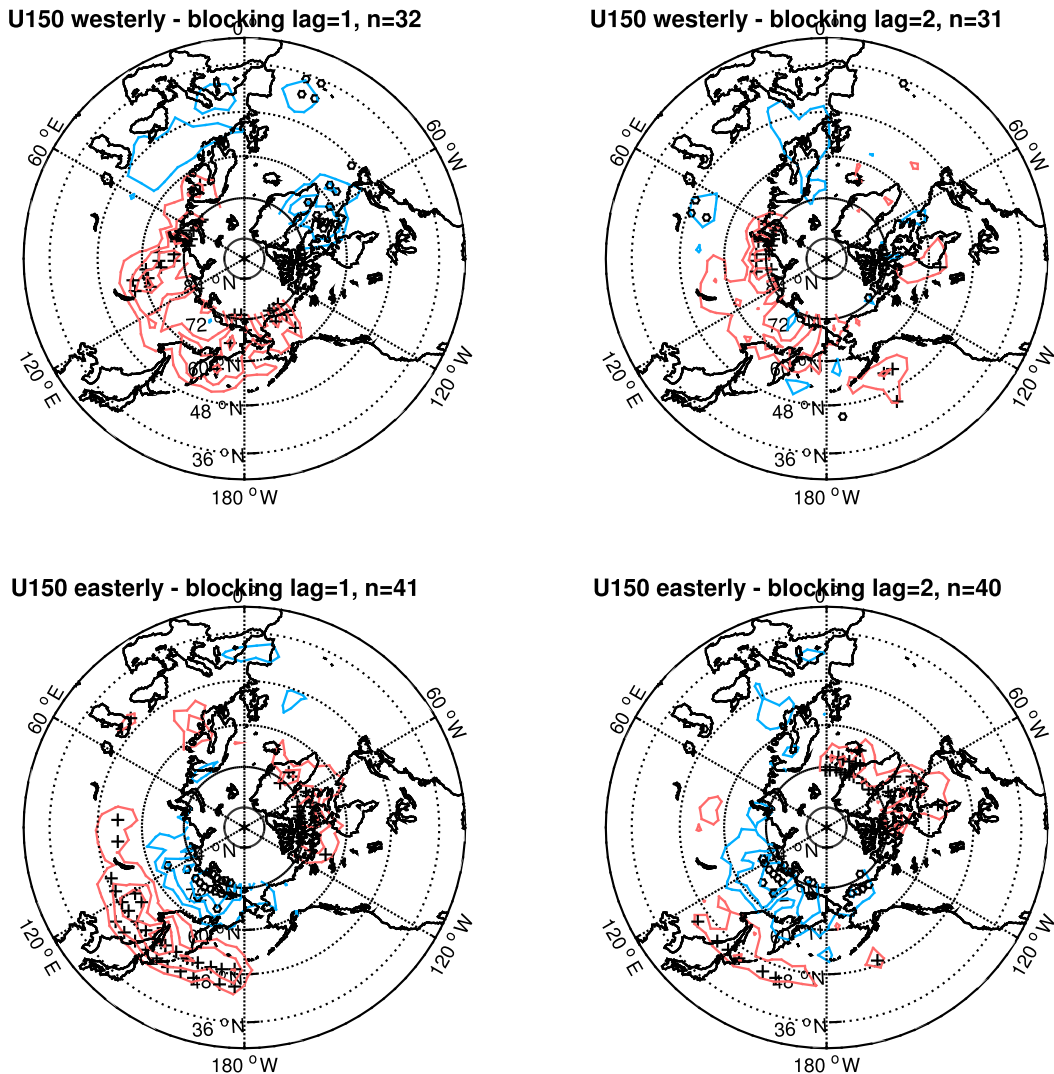


FIG. 7. Blocking frequency anomalies composited with respect to (top) westerly and (bottom) easterly anomalies in the daily  $[U150]_E$  index (see text), all for ERA data. (left) The composite blocking frequency anomaly averaged over days 3 to 7 after peaks of  $[U150]_E$  (lag 5); (right) as in (left), but for days 8 to 12. The numbers of peaks  $n$  used to calculate the composites are given in the titles of all panels. Contour interval is 4% and plus-circle symbols indicate significance as in Fig. 3.

and also consistent with Hinton et al. (2009). The large-scale circulation response to ENSO, namely, cyclonic anomalies over the North Pacific during El Niño (anticyclonic during La Niña), leads to decreased meridional gradients and higher potential for blocking (increased gradient and suppressed blocking during La Niña) on the northern flank of the anomaly. Over the lower and midlatitudes of the North Pacific, we only find weak and insignificant signals associated with ENSO, indicating enhanced (suppressed) blocking during La Niña (El Niño), agreeing with previous studies in the sign of the anomalies (e.g., Renwick and Wallace 1996; Wiedenmann et al. 2002). The relationship between

ENSO and blocking over Europe is weak, although there is some indication for NAO+-like blocking anomalies (see Woollings et al. 2008) during La Niña winters (i.e., decreased blocking over the western North Atlantic and increased blocking over southern Europe). The increased blocking over southern Europe during La Niña is also consistent with enhanced anticyclonic wave breaking during NAO+ (e.g., Martius et al. 2007).

Consistent with HMB16, the MJO is found to have a strong influence on blocking frequency variability all over the Northern Hemisphere. In particular, blocking frequency is decreased over the North Pacific after early

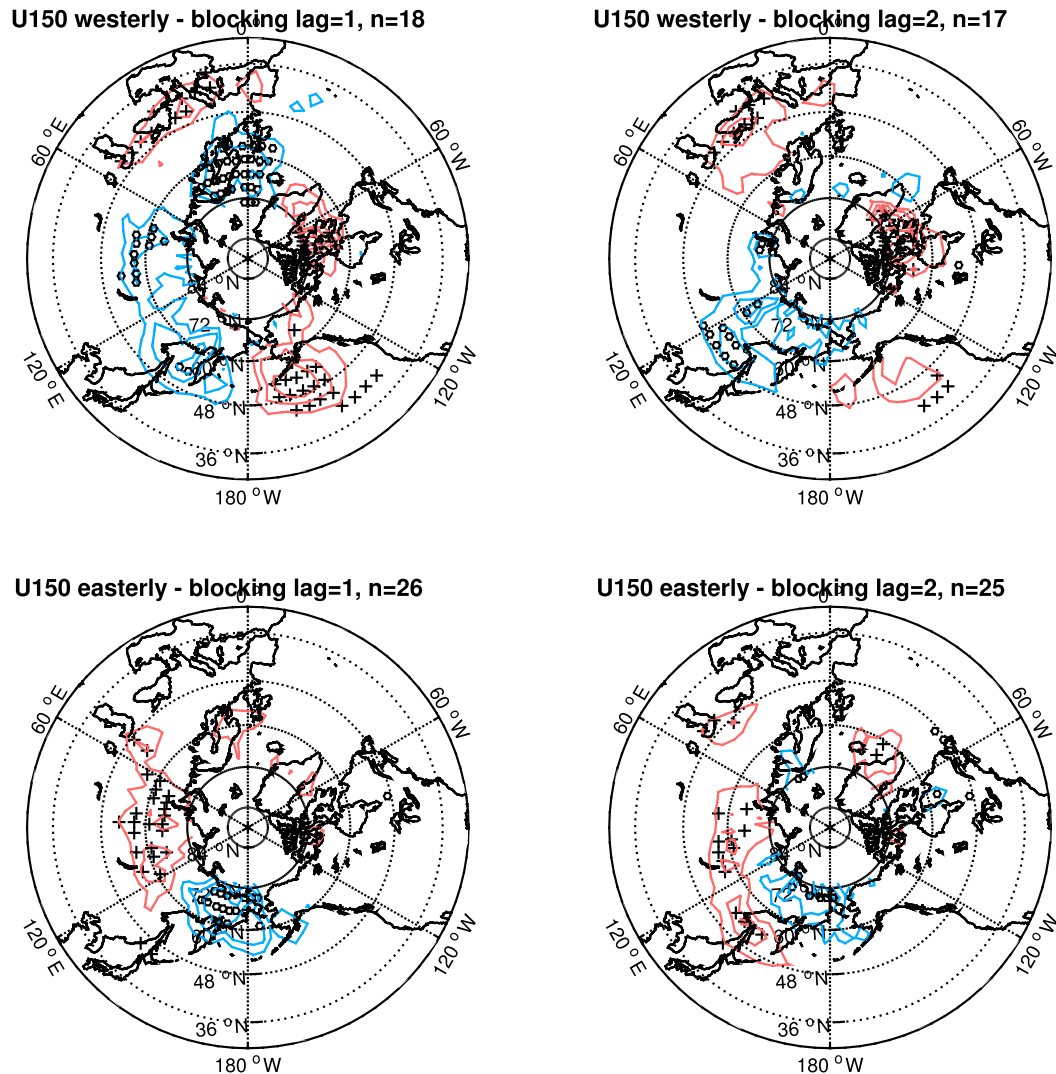


FIG. 8. As in Fig. 7, but for CLIM-TROPICS. Blocking anomalies are multiplied by a factor of 2 to give a similar amplitude compared to Fig. 7.

MJO phases (1–4), and blocking frequency is increased, especially over Europe, after late MJO phases (5–8). While our results are consistent with HMB16, we use a slightly different blocking index than HMB16 and also show model output that broadly confirms the results from the reanalysis.

Additionally, we investigate the case of a generally suppressed MJO and find, in the reanalysis, a significant increase in blocking frequency, especially over central and eastern Europe, an example of which is the winter of 1962/63 when the MJO was suppressed throughout the winter and a persistent blocking episode occurred over Europe leading to extremely low temperatures (Greatbatch et al. 2015). A suppressed MJO is associated with precipitation close to climatology (i.e., a zonally asymmetric dipole along the equator in the MJO

region; e.g., Adler et al. 2003) and easterly  $[U150]_E$  anomalies (Gollan and Greatbatch 2015). While the precipitation anomalies associated with MJO phase 6 project onto the climatological precipitation, thereby enhancing the zonal dipole, the similarity between the blocking response to the suppressed MJO and the blocking response to MJO phase 6 suggest that the zonal dipole in diabatic heating is important for this response. On the other hand, in the reanalysis, the blocking response to a suppressed MJO is similar to the response to easterly  $[U150]_E$  anomalies.

For  $[U150]_E$ , the most robust blocking signal was found in the high-latitude western North Pacific, where an increase (decrease) in blocking frequency is associated with the westerly (easterly) phase of  $[U150]_E$ . This finding, also being confirmed on pentad time scales, can

TABLE 1. Summary of the statistically significant blocking anomalies associated with the tropical modes under investigation in this study. Subtropical to midlatitudes (sub) are defined as the range 30°–48°N and mid- to high latitudes (high) are defined as the range 48°–72°N. Plus (+) signs indicate enhanced blocking, circles indicate decreased blocking, and Minus (–) signs indicates no change, while no differentiation is made between time scales. Asterisks mark agreement between reanalysis and relaxation experiment, and for the MJO, a signal for early (late) phases has to agree for at least 2 out of phases 1–4 (5–8) to be noted here. Results that contrast with previous results are marked with square brackets, and novel results are marked with curly brackets.

		Niño-3.4		MJO			$[U150]_E$	
		Warm	Cold	Early	Late	Suppressed	Westerly	Easterly
Pacific	Sub	–	–	–	–	–	–	–
140°E–120°W	High	[+*]	[o*]	o*	+	–	{+}	{o}
Atlantic	Sub	–	–	o	+	–	–	–
90°W–10°W	High	–	o	o	+	–	–	{+}
Central Europe	Sub	–	+	o	+	{+}	–	–
10°W–40°E	High	–	–	–	+	{+}	{o*}	{+*}

be explained by the influence of  $[U150]_E$  on the Rossby waveguide over the North Pacific: during easterly  $[U150]_E$ , the North Pacific waveguide is strengthened (see Fig. 8 in Gollan and Greatbatch 2015) and can guide Rossby waves away from the North Pacific, whereas during westerly  $[U150]_E$  the North Pacific waveguide is weakened so that Rossby waves are more likely to dissipate over the North Pacific, leading to blocking (Takaya and Nakamura 2001). Consistently, we have identified enhanced blocking frequency over northern Europe associated with the easterly phase of  $[U150]_E$ , on monthly mean and on pentad time scales, in the reanalysis (albeit weak in the reanalysis on pentad time scales) as well as in the tropical relaxation experiment, similar to the blocking anomalies associated with a suppressed MJO. However, there is dissimilarity between the European blocking anomalies associated with easterly  $[U150]_E$  and with early MJO phases that had been recognized as a driver for the easterly phase of  $[U150]_E$  (see Fig. 5 in Gollan and Greatbatch 2015). This supports the hypothesis that  $[U150]_E$  is not solely forced by the MJO, with meridional shifts of the ITCZ being a candidate (see Fig. 6 in Gollan and Greatbatch 2015).

The decrease in blocking frequency over the northern North Pacific, as found for the easterly phase of  $[U150]_E$ , occurs in a similar region where Woollings et al. (2010) identified a lack of blocking preceding weak stratospheric vortex regimes (i.e., increased likelihood for SSWs), raising the question as to whether the “stratospheric bridge” is playing a role for the blocking anomalies over Europe associated with  $[U150]_E$ . However, SSWs<sup>14</sup> that are important for the downward impact onto the European sector (Ineson and Scaife 2009; Bell et al. 2009) occur with a similar frequency when

comparing winters characterized by an easterly or a westerly  $[U150]_E$  in the ERA reanalysis. In the model, SSW frequency is slightly enhanced for easterly  $[U150]_E$  winters (about 0.65 per winter) compared to westerly  $[U150]_E$  winters (about 0.5 per winter), but easterly  $[U150]_E$  winters themselves are not statistically distinguishable from neutral  $[U150]_E$  winters in terms of SSW frequency.

Overall, our results underline the importance of a realistic representation of tropical dynamics in forecasting and climate models. In particular, a good representation of the MJO on intraseasonal to interannual time scales is important; indeed we have seen here the influence of MJO and  $[U150]_E$ . In this context, Scaife et al. (2016) have noted the importance of the tropics in the success of Met Office seasonal predictions. When interseasonal to decadal forecasts are considered, a proper initialization of the model is necessary to capture the phasing of ENSO to make use of its impacts onto the extratropics (e.g., Ding et al. 2013). The results of the present paper could also be used to empirically predict the tendency of blocking frequency in the Northern Hemisphere on different time scales. Apart from this, more work is needed to understand the mechanisms of how the tropical modes under investigation impact blocking—especially over Europe.

*Acknowledgments.* We want to thank three anonymous reviewers for helpful comments that substantially improved the manuscript. Also, many thanks to the ECMWF for the provision of the model used and computer facilities through an ECMWF Special Project. Thanks also to Prof. Dr. Thomas Jung who carried out the model runs reported here. Support from the German Ministry for Education (BMBF) through MiKlip2, subproject 01LP1517D (ATMOS-MODINI), is also gratefully acknowledged, as is support from the GEOMAR Helmholtz Centre for Ocean Research Kiel. Model data

<sup>14</sup>SSWs are measured by the algorithm of Charlton and Polvani (2007).

used in this paper and script for the calculation of the blocking index are available at <http://data.geomar.de>.

## REFERENCES

- Adames, Á. F., and J. M. Wallace, 2014: Three-dimensional structure and evolution of the MJO and its relation to the mean flow. *J. Atmos. Sci.*, **71**, 2007–2026, doi:10.1175/JAS-D-13-0254.1.
- Adler, R. F., and Coauthors, 2003: The Version-2 Global Precipitation Climatology Project (GPCP) monthly precipitation analysis (1979–present). *J. Hydrometeor.*, **4**, 1147–1167, doi:10.1175/1525-7541(2003)004<1147:TVGPCP>2.0.CO;2.
- Ayarzagüena, B., Y. J. Orsolini, U. Langematz, J. Abalichin, and A. Kubin, 2015: The relevance of the location of blocking highs for stratospheric variability in a changing climate. *J. Climate*, **28**, 531–549, doi:10.1175/JCLI-D-14-00210.1.
- Bao, M., and D. L. Hartmann, 2014: The response to MJO-like forcing in a nonlinear shallow-water model. *Geophys. Res. Lett.*, **41**, 1322–1328, doi:10.1002/2013GL057683.
- Barnes, E. A., E. Dunn-Sigouin, G. Masato, and T. Woollings, 2014: Exploring recent trends in Northern Hemisphere blocking. *Geophys. Res. Lett.*, **41**, 638–644, doi:10.1002/2013GL058745.
- Barriopedro, D., and N. Calvo, 2014: On the relationship between ENSO, stratospheric sudden warmings, and blocking. *J. Climate*, **27**, 4704–4720, doi:10.1175/JCLI-D-13-00770.1.
- , R. García-Herrera, A. R. Lupo, and E. Hernández, 2006: A climatology of Northern Hemisphere blocking. *J. Climate*, **19**, 1042–1063, doi:10.1175/JCLI3678.1.
- Bell, C. J., L. J. Gray, J. Charlton-Perez, M. M. Joshi, and A. Scaife, 2009: Stratospheric communication of El Niño teleconnections to European winter. *J. Climate*, **22**, 4083–4096, doi:10.1175/2009JCLI2717.1.
- Berrisford, P., B. J. Hoskins, and E. Tyrlis, 2007: Blocking and Rossby wave breaking on the dynamical tropopause in the Southern Hemisphere. *J. Atmos. Sci.*, **64**, 2881–2898, doi:10.1175/JAS3984.1.
- Brönnimann, S., 2007: Impact of El Niño–Southern Oscillation on European climate. *Rev. Geophys.*, **45**, RG3003, doi:10.1029/2006RG000199.
- Cassou, C., 2008: Intraseasonal interaction between the Madden–Julian oscillation and the North Atlantic Oscillation. *Nature*, **455**, 523–527, doi:10.1038/nature07286.
- Charlton, A. J., and L. M. Polvani, 2007: A new look at stratospheric sudden warmings. Part I: Climatology and modeling benchmarks. *J. Climate*, **20**, 449–469, doi:10.1175/JCLI3996.1.
- Croci-Maspoli, M., and H. C. Davies, 2009: Key dynamical features of the 2005/06 European winter. *Mon. Wea. Rev.*, **137**, 664–678, doi:10.1175/2008MWR2533.1.
- Dahlke, S., 2015: Global teleconnections due to diabatic heating associated with local rainfall events. M.S. thesis, Faculty of Mathematics and Natural Sciences, Christian-Albrechts-Universität zu Kiel, 73 pp.
- Dee, D. P., E. Källén, A. J. Simmons, and L. Haimberger, 2011: Comments on “Reanalyses suitable for characterizing long-term trends.” *Bull. Amer. Meteor. Soc.*, **92**, 65–70, doi:10.1175/2010BAMS3070.1.
- Ding, H., R. J. Greatbatch, M. Latif, W. Park, and R. Gerdes, 2013: Hindcast of the 1976/77 and 1998/99 climate shifts in the Pacific. *J. Climate*, **26**, 7650–7661, doi:10.1175/JCLI-D-12-00626.1.
- Ferranti, L., T. N. Palmer, F. Molteni, and E. Klinker, 1990: Tropical–extratropical interaction associated with the 30–60 day oscillation and its impact on medium and extended range prediction. *J. Atmos. Sci.*, **47**, 2177–2199, doi:10.1175/1520-0469(1990)047<2177:TEIAWT>2.0.CO;2.
- Garfinkel, C. I., and D. L. Hartmann, 2008: Different ENSO teleconnections and their effects on the stratospheric polar vortex. *J. Geophys. Res.*, **113**, D18114, doi:10.1029/2008JD009920.
- , —, and F. Sassi, 2010: Tropospheric precursors of anomalous Northern Hemisphere stratospheric polar vortices. *J. Climate*, **23**, 3282–3299, doi:10.1175/2010JCLI3010.1.
- , A. H. Butler, D. W. Waugh, M. M. Hurwitz, and L. M. Polvani, 2012a: Why might stratospheric sudden warmings occur with similar frequency in El Niño and La Niña winters? *J. Geophys. Res.*, **117**, D19106, doi:10.1029/2012JD017777.
- , S. B. Feldstein, D. W. Waugh, C. Yoo, and S. Lee, 2012b: Observed connection between stratospheric sudden warmings and the Madden-Julian oscillation. *Geophys. Res. Lett.*, **39**, L18807, doi:10.1029/2012GL053144.
- , M. M. Hurwitz, D. W. Waugh, and A. H. Butler, 2013: Are the teleconnections of central Pacific and eastern Pacific El Niño distinct in boreal wintertime? *Climate Dyn.*, **41**, 1835–1852, doi:10.1007/s00382-012-1570-2.
- , J. J. Benedict, and E. D. Maloney, 2014: Impact of the MJO on the boreal winter extratropical circulation. *Geophys. Res. Lett.*, **41**, 6055–6062, doi:10.1002/2014GL061094.
- Gollan, G., and R. J. Greatbatch, 2015: On the extratropical influence of variations of the upper-tropospheric equatorial zonal-mean zonal wind during boreal winter. *J. Climate*, **28**, 168–185, doi:10.1175/JCLI-D-14-00185.1.
- , —, and T. Jung, 2015: Origin of variability in Northern Hemisphere winter blocking on interannual to decadal time scales. *Geophys. Res. Lett.*, **42**, 10 037–10 046, doi:10.1002/2015GL066572.
- Greatbatch, R. J., G. Gollan, T. Jung, and T. Kunz, 2012: Factors influencing Northern Hemisphere winter mean atmospheric circulation anomalies during the period 1960/61 to 2001/02. *Quart. J. Roy. Meteor. Soc.*, **138**, 1970–1982, doi:10.1002/qj.1947.
- , —, —, and —, 2015: Tropical origin of the severe European winter of 1962/1963. *Quart. J. Roy. Meteor. Soc.*, **141**, 153–165, doi:10.1002/qj.2346.
- Hansen, F., R. J. Greatbatch, G. Gollan, T. Jung, and A. Weisheimer, 2017: Remote control of North Atlantic Oscillation predictability via the stratosphere. *Quart. J. Roy. Meteor. Soc.*, **143**, 706–719, doi:10.1002/qj.2958.
- Henderson, S. A., E. D. Maloney, and E. A. Barnes, 2016: The influence of the Madden–Julian oscillation on Northern Hemisphere winter blocking. *J. Climate*, **29**, 4597–4616, doi:10.1175/JCLI-D-15-0502.1.
- Hinton, T. J., B. J. Hoskins, and G. M. Martin, 2009: The influence of tropical sea surface temperatures and precipitation on North Pacific atmospheric blocking. *Climate Dyn.*, **33**, 549–563, doi:10.1007/s00382-009-0542-7.
- Hoskins, B. J., M. E. McIntyre, and A. W. Robertson, 1985: On the use and significance of isentropic potential vorticity maps. *Quart. J. Roy. Meteor. Soc.*, **111**, 877–946, doi:10.1002/qj.49711147002.
- Ineson, S., and A. A. Scaife, 2009: The role of the stratosphere in the European climate response to El Niño. *Nat. Geosci.*, **2**, 32–36, doi:10.1038/ngeo381.
- Jung, T., M. J. Miller, and T. N. Palmer, 2010: Diagnosing the origin of extended-range forecast errors. *Mon. Wea. Rev.*, **138**, 2434–2446, doi:10.1175/2010MWR3255.1.
- Kraucunas, I., and D. L. Hartmann, 2005: Equatorial superrotation and the factors controlling the zonal-mean zonal winds in the



- tropical upper troposphere. *J. Atmos. Sci.*, **62**, 371–389, doi:10.1175/JAS-3365.1.
- Lee, S., S.-W. Son, K. Grise, and S. B. Feldstein, 2007: A mechanism for the poleward propagation of zonal mean flow anomalies. *J. Atmos. Sci.*, **64**, 849–868, doi:10.1175/JAS3861.1.
- L'Heureux, M. L., and R. W. Higgins, 2008: Boreal winter links between the Madden–Julian oscillation and the Arctic Oscillation. *J. Climate*, **21**, 3040–3050, doi:10.1175/2007JCLI1955.1.
- , and D. W. J. Thompson, 2006: Observed relationships between the El Niño–Southern Oscillation and the extratropical zonal-mean circulation. *J. Climate*, **19**, 276–287, doi:10.1175/JCLI3617.1.
- Lin, H., G. Brunet, and J. Derome, 2009: An observed connection between the North Atlantic Oscillation and the Madden–Julian oscillation. *J. Climate*, **22**, 364–380, doi:10.1175/2008JCLI2515.1.
- , —, and B. Yu, 2015: Interannual variability of the Madden–Julian Oscillation and its impact on the North Atlantic Oscillation in the boreal winter. *Geophys. Res. Lett.*, **42**, 5571–5576, doi:10.1002/2015GL064547.
- Martius, O., C. Schwierz, and H. C. Davies, 2007: Breaking waves at the tropopause in the wintertime Northern Hemisphere: Climatological analyses of the orientation and the theoretical lc1/2 classification. *J. Atmos. Sci.*, **64**, 2576–2592, doi:10.1175/JAS3977.1.
- , L. M. Polvani, and H. C. Davies, 2009: Blocking precursors to stratospheric sudden warming events. *Geophys. Res. Lett.*, **36**, L14806, doi:10.1029/2009GL038776.
- Oliver, E. C. J., 2016: Blind use of reanalysis data: Apparent trends in Madden–Julian oscillation activity driven by observational changes. *Int. J. Climatol.*, **36**, 3458–3468, doi:10.1002/joc.4568.
- Pelly, J. L., and B. J. Hoskins, 2003: A new perspective on blocking. *J. Atmos. Sci.*, **60**, 743–755, doi:10.1175/1520-0469(2003)060<0743:ANPOB>2.0.CO;2.
- Renwick, J. A., and J. M. Wallace, 1996: Relationships between North Pacific wintertime blocking, El Niño, and the PNA pattern. *Mon. Wea. Rev.*, **124**, 2071–2076, doi:10.1175/1520-0493(1996)124<2071:RBNPWB>2.0.CO;2.
- Scaife, A. A., and Coauthors, 2016: Tropical rainfall, Rossby waves and regional winter climate predictions. *Quart. J. Roy. Meteor. Soc.*, **44**, 1–11, doi:10.1002/qj.2910.
- Scherrer, S. C., M. Croci-Maspoli, C. Schwierz, and C. Appenzeller, 2006: Two-dimensional indices of atmospheric blocking and their statistical relationship with winter climate patterns in the Euro-Atlantic region. *Int. J. Climatol.*, **26**, 233–249, doi:10.1002/joc.1250.
- Schwierz, C., M. Croci-Maspoli, and H. C. Davies, 2004: Perspicacious indicators of atmospheric blocking. *Geophys. Res. Lett.*, **31**, L06125, doi:10.1029/2003GL019341.
- Sillmann, J., and M. Croci-Maspoli, 2009: Present and future atmospheric blocking and its impact on European mean and extreme climate. *Geophys. Res. Lett.*, **36**, L10702, doi:10.1029/2009GL038259.
- Takaya, K., and H. Nakamura, 2001: A formulation of a phase-independent wave-activity flux for stationary and migratory quasigeostrophic eddies on a zonally varying basic flow. *J. Atmos. Sci.*, **58**, 608–627, doi:10.1175/1520-0469(2001)058<0608:AFOAPI>2.0.CO;2.
- Tibaldi, S., and F. Molteni, 1990: On the operational predictability of blocking. *Tellus*, **42A**, 343–365, doi:10.3402/tellusa.v42i3.11882.
- Trenberth, K. E., G. W. Branstator, D. Karoly, A. Kumar, N.-C. Lau, and C. Ropelewski, 1998: Progress during TOGA in understanding and modeling global teleconnections associated with tropical sea surface temperatures. *J. Geophys. Res.*, **103**, 14 291–14 324, doi:10.1029/97JC01444.
- Trigo, R. M., I. F. Trigo, C. C. DaCamara, and T. J. Osborn, 2004: Climate impact of the European winter blocking episodes from the NCEP/NCAR reanalyses. *Climate Dyn.*, **23**, 17–28, doi:10.1007/s00382-004-0410-4.
- Uppala, S. M., and Coauthors, 2005: The ERA-40 Re-Analysis. *Quart. J. Roy. Meteor. Soc.*, **131**, 2961–3012, doi:10.1256/qj.04.176.
- Wheeler, M. C., and H. H. Hendon, 2004: An all-season real-time multivariate MJO index: Development of an index for monitoring and prediction. *Mon. Wea. Rev.*, **132**, 1917–1932, doi:10.1175/1520-0493(2004)132<1917:AARMMI>2.0.CO;2.
- Wiedemann, J. M., A. R. Lupo, I. I. Mokhov, and E. A. Tikhonova, 2002: The climatology of blocking anticyclones for the Northern and Southern Hemispheres: Block intensity as a diagnostic. *J. Climate*, **15**, 3459–3473, doi:10.1175/1520-0442(2002)015<3459:TCOBAF>2.0.CO;2.
- Woollings, T., B. Hoskins, M. Blackburn, and P. Berrisford, 2008: A new Rossby wave-breaking interpretation of the North Atlantic Oscillation. *J. Atmos. Sci.*, **65**, 609–626, doi:10.1175/2007JAS2347.1.
- , A. Charlton-Perez, S. Ineson, A. G. Marshall, and G. Masato, 2010: Associations between stratospheric variability and tropospheric blocking. *J. Geophys. Res.*, **115**, D06108, doi:10.1029/2009JD012742.
- Yoo, C., S. Lee, and S. B. Feldstein, 2012a: Arctic response to an MJO-like tropical heating in an idealized GCM. *J. Atmos. Sci.*, **69**, 2379–2393, doi:10.1175/JAS-D-11-0261.1.
- , —, and —, 2012b: Mechanisms of Arctic surface air temperature change in response to the Madden–Julian oscillation. *J. Climate*, **25**, 5777–5790, doi:10.1175/JCLI-D-11-00566.1.
- Zhou, S., and A. J. Miller, 2005: The interaction of the Madden–Julian oscillation and the Arctic Oscillation. *J. Climate*, **18**, 143–159, doi:10.1175/JCLI3251.1.